Available online at www.sciencedirect.com
SCIENCE DIRECT®
OCEAN ENGINEERING
Ocean Engineering 33 (2006) 1373–1400
www.elsevier.com/locate/oceaneng

Time-domain numerical simulation of ocean cable structures

J.I. Gobat [a], M.A. Grosenbaugh [b,*]

[a] *Applied Physics Laboratory, University of Washington, Seattle, WA 98105, USA*
[b] *Department of Applied Physics and Engineering, Woods Hole Oceanographic Institution, Woods Hole, MA 02543, USA*

Received 2 February 2005; accepted 13 July 2005
Available online 15 November 2005

Abstract

This paper describes the numerical features of WHOI Cable, a computer program for analyzing the statics and dynamics of oceanographic cable structures. The governing equations include the effects of geometric and material nonlinearities, bending stiffness for seamless modeling of slack cables, and a model for the interaction of cable segments with the sea floor. The program uses the generalized-α time integration algorithm, adaptive time stepping, and adaptive spatial gridding to produce accurate, stable solutions for dynamic problems. The nonlinear solver uses adaptive relaxation to improve robustness for both static and dynamic problems. The program solves surface and subsurface single-point mooring problems, multi-leg and branched array systems, and towing and drifting problems. User specified forcing can include waves, currents, wind, and ship speed.
© 2005 Elsevier Ltd. All rights reserved.

Keywords: Cable dynamics; Mooring dynamics; Towed systems

1. Introduction

The purpose of this paper is to present a new computer program for analyzing the nonlinear dynamics of ocean cable structures. The governing equations include the effects of geometric and material nonlinearities, bending stiffness for seamless modeling of slack cables, and a model for the interaction of cable segments with the sea floor. The main

* Corresponding author. Fax: +1 508 289 2191.
E-mail address: mgrosenbaugh@whoi.edu (M.A. Grosenbaugh).

0029-8018/$ - see front matter © 2005 Elsevier Ltd. All rights reserved.
doi:10.1016/j.oceaneng.2005.07.012

feature of the program is a novel time integration algorithm that produces accurate, stable, and robust solutions to dynamic problems. The algorithm extends classical finite difference schemes (Ablow and Schechter, 1983; Howell, 1992; Koh et al., 1999) that have become popular for solving ocean towing and mooring problems. The new algorithm provides a family of time integration schemes that include these classical treatments. This gives us the ability to directly compare our new formulation to the previous methods.

Finite difference methods are not the only means for solving undersea cable problems. Other methods can be distinguished principally from the way in which they discretize the physical system in space. These other methods include lumped parameters and finite elements. While there is more universal agreement on the temporal discretization schemes (most use finite differences), there is some variation in the way that the temporally discretized equations of the different methods are integrated in time. Beyond these distinctions are the mathematical and physical features incorporated by the various methods such as bending stiffness, seabed interaction effects, and treatment of vortex-induced vibrations. Below is a brief historical description of modern undersea cable dynamics methods including the development of finite difference methods that form the basis for the formulation presented in this paper.

1.1. Spatial discretization

Walton and Polachek (1960) published the first treatment of the dynamic solution that resembles very closely the solution methods in use today. They formulated the equations of motion for discrete elements and used centered finite differences to discretize the time derivative terms. With the addition of cable extensibility by Polachek et al. (1963) there existed a remarkably complete treatment of the nonlinear time domain problem. This first solution, using a force balance on discrete elements to write the equations of motion, is what we now categorize as a lumped parameter method. The terminology arises from the lumping of the mass and externally applied forces at adjacent nodes, which are joined by mass-less springs. This discretization approach has an intuitive simplicity to it and as such is relatively easy to implement. Notable models that make use of this approach are described by Delmer et al. (1983); Huang (1994); Thomas (1993), and Thomas and Hearn (1994). Buckham and Nahon (2001) have recently incorporated bending stiffness into a lumped parameter model for low-tension ROV tethers.

Finite element methods derive their governing equations through principles of virtual work. One advantage of this approach is the possibility of a more sophisticated treatment of mass. Whereas lumped parameter derivations must necessarily place all mass at discrete nodes, finite element methods can derive the governing equations using an integration of the mass over the entire element, thus leading to a ‘consistent’ mass formulation (Leonard and Nath, 1981). The starting point for finite element methods as applied to the marine cable problem is typically a discrete element, much like the lumped parameter methods. Examples of such derivations include Engseth et al. (1988); McNamara et al. (1986), and Zueck (1997). Paulling and Webster (1986), following Garrett (1982), take the alternative approach of formulating differential equations of motion that are solved by the substitution of a discrete collection of shape functions which minimize the element energy.

The majority of state-of-the-art programs currently used for riser modeling is based on finite elements and, in most cases, includes the effects of bending (Larsen, 1992).

A third approach, which we have adopted for this paper, is to write the continuous partial differential equations and then apply a spatial discretization scheme based on finite differences. We distinguish between this and lumped parameter methods based on the starting point, which is an infinitesimally small differential element as compared to a finite discrete element used for the lumped parameter case. Given similar physical assumptions, the two methods are entirely equivalent as demonstrated by Huang (1994). An early application of this approach to marine cables was due to Ablow and Schechter (1983). Their method was later adapted by a number of authors (Howell, 1992; Burgess, 1993; Tjavaras, 1996) to account for the effects of bending. The model development detailed in Section 2 of this paper is based on these later approaches.

Finally, a few alternatives to the spatial discretizations outlined above have appeared in the literature. Chiou and Leonard (1991); Sun et al. (1994) describe the 'direct integration method', whereby a boundary value problem is recast as a set of initial value problems. Each initial value problem is integrated spatially from a boundary with known boundary conditions. The solutions from these integrations are combined to form a total solution that satisfies all boundary conditions. Because the initial value approach allows for explicit numerical integration in space, the method has the advantage that the solution of large linear systems of equations, typical of implicit finite difference and finite element schemes, can be avoided. There is, of course, a spatial discretization implied by the numerical integration of the transformed governing equations. Sun et al. (1994) point out the need for a method to suppress any spurious solution components that may grow as the spatial integrations proceed along the cable. Another alternative scheme is collocation, which breaks the cable into a small number of segments and fits high order Chebyshev polynomials as a solution to the governing equations over each region (Chatjigeorgiou and Mavrakos, 1999).

1.2. Temporal discretization

For all spatial discretization methods, the resulting equations are typically written as a nonlinear matrix equation known as the semi-discrete equation of motion, because the time derivatives of the vector of dependent variables are left as continuous functions. The exception to this procedure is in finite difference based solutions, which typically are differenced both in space and in time as part of the same process. This leads to yet another distinction between lumped parameter and finite difference approaches. The starting point for a finite difference method is typically a set of first-order hyperbolic partial differential equations. The equations of motion for lumped parameter schemes are most often presented in matrix form as a system of second-order ordinary differential equations—the semi-discrete equation of motion.

Most temporal integration schemes in use today have their roots in the method developed by Newmark (1959). Hughes and Belytschko (1983) provide a summary of the development of these types of methods in the context of linear finite element structural dynamics. The methods typically employ temporal finite differences, with a variety of different schemes used to interpolate the solution over the time step. Most methods can now be cast into unified multi-parameter integration schemes where an adjustment in the parameters leads to one of several different methods with different numerical properties (e.g., Hoff and Pahl, 1988; Wood, 1990; Zienkiewicz et al., 1984). Thomas (1993) studied the three 'classic' methods (Newmark, Houbolt, and Wilson-θ) and their applicability to the mooring dynamics problem. He concluded that Houbolt was the best choice. Park (1975) noted earlier that Houbolt was a good choice for highly nonlinear problems.

In addition to Newmark and its variants, which are popularly employed with finite element based models, researchers in the cable dynamics field have employed a variety of different schemes for the temporal integration problem. Chiou and Leonard (1991) use simple backward finite differences. Sun et al. (1994) use the generalized trapezoidal rule, which is a first-order variant of the Newmark method. Paulling and Webster (1986) used the Adams–Moulton method, which in first-order form reduces to the trapezoidal rule. Sanders (1982) used a computationally expensive but fourth-order accurate Runge–Kutta procedure. This is unusual in that most researchers have accepted first- or second-order accuracy to reduce computational expense.

A popular finite difference scheme is the second-order accurate box method, in which the governing equations are discretized on the half-grid point in both space and time. This method was first employed for the solution of tow cable dynamics by Ablow and Schechter (1983). Since then it has been employed in both towing and mooring applications by Milinazzo et al. (1987); Howell (1992); Tjavaras (1996); Chatjigeorgiou and Mavrakos (1999), and Park et al. (2003) among others. As will be shown, the temporal portion of the box method is a special form of the generalized-α method (Chung and Hulbert, 1993; Gobat and Grosenbaugh, 2001a), which forms the framework of the temporal discretization scheme used in this paper. This development will also demonstrate that the box method is seldom the best choice of temporal discretization schemes for the cable dynamics problem. In a recent paper, Koh et al. (1999) came to this same conclusion and proposed a first-order accurate modified box method that used backward differences for the temporal discretization. This method is also a special form of the generalized-α method that we have implemented.

In the next section, we present the governing equations for the two-dimensional dynamics of undersea cables. This is followed by a description, in Section 3, of the spatial discretization scheme used in this paper. The generalized-α temporal integration method is presented in Section 4. Boundary conditions are given in Section 5. This is followed by a discussion of our nonlinear solver, which uses nonlinear relaxation with adaptive techniques to improve robustness. Finally, in Section 7, we present the results from three test problems, concentrating on results obtained from using different time-integration schemes.

2. Governing equations

The WHOI Cable program includes governing equations for both two- and three-dimensional models. For succinctness, only the two-dimensional equations (Howell, 1992) are discussed in this section. The derivation of the three-dimensional equations is presented in Tjavaras (1996). The equations of motion for the dynamic problem in two-dimensions are (Gobat, 2000):

$$T'(\varepsilon)\frac{\partial \varepsilon}{\partial s} - S_n\frac{\partial \phi}{\partial s} - m\frac{\partial u}{\partial t} + mv\frac{\partial \phi}{\partial t} - w_o \cos\phi - \frac{1}{2}\rho_w d\pi C_{dt} u_r|u_r|\sqrt{1+\varepsilon} = 0 \tag{1}$$

$$\frac{\partial S_n}{\partial s} + T(\varepsilon)\frac{\partial \phi}{\partial s} - (m+m_a)\frac{\partial v}{\partial t} - \left[mu + \left(\frac{1}{4}\rho_w \pi d + m_a\right)(U\cos\phi + V\sin\phi)\right]\frac{\partial \phi}{\partial t}$$
$$+ w_o \sin\phi - \frac{1}{2}\rho_w d C_{dn} v_r|v_r|\sqrt{1+\varepsilon} = 0 \tag{2}$$

$$\frac{\partial u}{\partial s} - v\frac{\partial \phi}{\partial s} - \frac{\partial \varepsilon}{\partial t} = 0 \tag{3}$$

$$\frac{\partial v}{\partial s} + u\frac{\partial \phi}{\partial s} - (1+\varepsilon)\frac{\partial \phi}{\partial t} = 0 \tag{4}$$

$$\frac{\partial \phi}{\partial s} - \Omega_3 = 0 \tag{5}$$

$$EI\frac{\partial \Omega_3}{\partial s} + S_n(1+\varepsilon)^3 = 0 \tag{6}$$

The independent variables are s, the Lagrangian coordinate measured along the unstretched cable, and t, time. Other variables are:

ε	strain
$T(\varepsilon)$	effective tension as a function of strain
$T'(\varepsilon)$	first derivative of the effective tension with respect to strain
S_n	shear force
u, v	cable velocity in the normal and tangential directions
U, V	current velocity in the vertical and horizontal directions
u_r, v_r	cable velocity in the normal and tangential directions relative to current
ϕ	cable inclination from the vertical
Ω_3	cable curvature
C_{dn}, C_{dt}	cable normal and tangential drag coefficients
m	cable mass per length
m_a	cable added mass per length
w_o	cable wet weight per length
ρ_w	density of sea water

By defining $\mathbf{Y} = [\varepsilon, S_n, u, v, \phi, \Omega_3]^{\mathrm{T}}$, (1-6) can be written in matrix form as

$$\mathbf{M}\frac{\partial \mathbf{Y}}{\partial t} + \mathbf{K}\frac{\partial \mathbf{Y}}{\partial s} + \mathbf{F}(\mathbf{Y}, s, t) = 0 \tag{7}$$

The continuous forms of the mass matrix, stiffness matrix, and forcing vector are

$$\mathbf{M} = \begin{bmatrix} 0 & 0 & -m & 0 & mv & 0 \\ 0 & 0 & 0 & -(m+m_a) & -\left[mu + \left(\frac{1}{4}\rho_w \pi d + m_a\right)(U\cos\phi + V\sin\phi)\right] & 0 \\ -1 & 0 & 0 & 0 & 0 & 0 \\ 0 & 0 & 0 & 0 & -(1+\varepsilon) & 0 \\ 0 & 0 & 0 & 0 & 0 & 0 \\ 0 & 0 & 0 & 0 & 0 & 0 \end{bmatrix} \tag{8}$$

$$\mathbf{K} = \begin{bmatrix} T/(\varepsilon) & 0 & 0 & 0 & S_n & 0 \\ 0 & 1 & 0 & 0 & T(\varepsilon) & 0 \\ 0 & 0 & 1 & 0 & -v & 0 \\ 0 & 0 & 0 & 1 & u & 0 \\ 0 & 0 & 0 & 0 & 1 & 0 \\ 0 & 0 & 0 & 0 & 0 & EI \end{bmatrix} \tag{9}$$

$$\mathbf{F} = \begin{bmatrix} -w_o \cos\phi - \frac{1}{2}\rho_w d\pi C_{dt} u_r |u_r| \sqrt{1+\varepsilon} \\ w_o \sin\phi - \frac{1}{2}\rho_w d C_{dn} v_r |v_r| \sqrt{1+\varepsilon} \\ 0 \\ 0 \\ -\Omega_3 \\ S_n(1+\varepsilon)^3 \end{bmatrix} \tag{10}$$

Note that the distribution of terms as either stiffness or force is somewhat arbitrary as spatial derivatives of ϕ could also appear as Ω_3. Experience has shown that the iterative nonlinear solver typically proceeds more quickly when any dependence on ϕ is explicitly incorporated into the equations of motion. The static governing equations can be derived from (1-6) simply by dropping time derivatives and velocity terms.

3. Spatial discretization

Unlike traditional box method solutions in which the governing equations are discretized in both space and time in one step, we have chosen to discretize the equations in two distinct steps. The spatial discretization used is the same as that in the box method: spatial derivatives are replaced by what look like traditional backward differences. Because the discretization is applied on the half-grid points, the method is second order accurate (Ablow and Schechter, 1983).

If there are n nodal points along the cable, then we can derive a set of $n-1$ matrix equations (one equation per half grid point) that can be written as:

$$\tilde{\mathbf{M}}_{j-(1/2)}\begin{bmatrix}\dot{\mathbf{Y}}_{j-1}\\ \dot{\mathbf{Y}}_{j}\end{bmatrix} + \tilde{\mathbf{K}}_{j-(1/2)}\begin{bmatrix}\mathbf{Y}_{j-1}\\ \mathbf{Y}_{j}\end{bmatrix} + \tilde{\mathbf{F}}_{j-(1/2)} = 0 \tag{11}$$

where the overdot signifies differentiation with respect to time and the subscript j defines the node number. The matrices $\tilde{\mathbf{M}}_{j-(1/2)}$ and $\tilde{\mathbf{K}}_{j-(1/2)}$ and the vector $\tilde{\mathbf{F}}_{j-(1/2)}$ are modified forms of (8-10), containing constants and variables associated with nodes j and $j-1$. The matrices and vector have dimensions $N\times 2N$ and $N\times 1$, respectively, where N is the number of dependent variables at each node ($N=6$ for two dimensions and $N=13$ for three dimensions). Two-dimensional forms of $\tilde{\mathbf{M}}_{j-(1/2)}$, $\tilde{\mathbf{K}}_{j-(1/2)}$, and $\tilde{\mathbf{F}}_{j-(1/2)}$ are given in Gobat and Grosenbaugh (2001a).

If we assemble the $n-1$ nodal matrices and vectors, along with appropriate boundary conditions, we can write the semi-discrete equation of motion for all of the dependent variables at all of the nodes as

$$\tilde{\mathbf{M}}\dot{Y} + \tilde{\mathbf{K}}Y + \tilde{\mathbf{F}} = 0 \tag{12}$$

This is similar to the assembly procedure common in finite element analysis. In this case, the pieces to be assembled are rectangular blocks of equations, which couple two adjacent nodes rather than square element stiffness and mass matrices.

In many moorings with low flexural stiffness, half-grid spatial discretization can lead to undesirable spatial oscillations in the solution. This phenomenon can be easily understood by considering (6), which relates shear force to curvature. This equation is spatially discretized as

$$2\,EI\left[\frac{\Omega_{3j}-\Omega_{3j-1}}{\Delta s_j}\right] + S_{nj}(1+\varepsilon_j)^3 + S_{nj}(1+\varepsilon_{j-1})^3 = 0 \tag{13}$$

If $EI\approx 0$ and $\varepsilon \ll 1$ as is typical, the only solution (barring $\Delta s_j=0$) is $S_{nj}\approx -S_{nj-1}$. If $|S_{nj}|>0$, the shear force will oscillate about zero from one node to the next. This error is particularly manifest in areas of high curvature and at the boundaries. Increasing the density of the spatial mesh minimizes this problem (Burgess, 1993). The most easily applied spatial discretization is uniform spacing given by

$$\Delta s_j = \frac{L}{n-1} \tag{14}$$

where L is the length of the cable segment and n is the number of nodes used in the discretization. Unfortunately, using a uniform mesh with small Δs to reduce spatial oscillations can require a large number of nodes. An alternative is to make the mesh finer only in problem areas—areas of high curvature and at the boundaries. To automate this allocation of nodes, we developed a procedure such that given a static solution based on a uniform mesh, we could optimize the mesh in some sense and then calculate the dynamic solution using the nonuniform mesh. The procedure, outlined below, is based on that described by Eggleton (1971). It is worth noting that Press et al. (1989) described a procedure, also based on the Eggleton approach, that adaptively refines the mesh as part of the nonlinear static solution procedure. That procedure had significant problems with convergence when applied to the geometrically nonlinear problems considered here. It also requires that three equations and additional dependent variables be added to the problem.

The approach to mesh refinement can be understood by considering a minimization of the sum given by

$$\sum_{j=2}^{n} \{c_w[\Omega_3(s_j) - \Omega_3(s_{j-1})] + (s_j - s_{j-1})\}^2 \tag{15}$$

The s_j coordinates of the n nodes are unknown, but, from our initial static solution (with uniform spacing), we can provide a good estimate of $\Omega_3(s)$ for any value of s. The first term in the sum will place nodes close together in areas of high variability in Ω_3. The second term will keep nodes from getting too far apart in areas of low variability in Ω_3. The constant, c_w, controls the weighting used to place nodes with respect to these two effects. For large c_w a large proportion of the n available nodes will be used in areas of high curvature with large spacing between the remaining nodes in other regions of the system. In contrast, a small c_w results in a nearly uniform mesh with little emphasis placed on refining mesh density in high curvature regions.

Minimizing (15) requires that we solve an n degree of freedom nonlinear least squares problem. Alternatively, we can approximate the sum as an integral and cast the minimization as a variational problem. If we define, the mesh control function

$$f(s) = c_w\Omega_3(s) + s \tag{16}$$

then (15) is simply

$$\sum_{j=2}^{n} |f(s_j) - f(s_{j-1})|^2 \tag{17}$$

Without affecting the solution of the minimization problem, we can introduce a new independent variable, q, which varies uniformly throughout the mesh (Δq is a constant), and rewrite the summation as

$$\sum_{j=2}^{n} \left[\frac{f(s_j) - f(s_{j-1})}{s_j - s_{j-1}}\right]^2 \frac{(s_j - s_{j-1})^2}{\Delta q} \tag{18}$$

We can approximate this sum as the integral given by

$$\int_0^L \left(\frac{\mathrm{d}f}{\mathrm{d}s}\right)^2 \frac{\mathrm{d}s}{\mathrm{d}q}\mathrm{d}s = \int_0^L \left(c_w \frac{\mathrm{d}\Omega_3}{\mathrm{d}s} + 1\right)^2 \frac{\mathrm{d}s}{\mathrm{d}q}\mathrm{d}s \tag{19}$$

We can then minimize the integral form by solving the variational problem

$$\delta \int_0^L [c_w \Omega_s'(s) + 1]^2 \frac{\mathrm{d}s}{\mathrm{d}q}\mathrm{d}s = 0 \tag{20}$$

In writing (20), we have substituted a normalized estimate of the curvature gradient, $\Omega_s'(s)$, for the spatial derivative of $\Omega_3(s)$. The estimate is defined as

$$\Omega_{sj}' = \frac{|\Omega_{3j} - \Omega_{3j-1}|}{\max|\Omega_{3k} - \Omega_{3k-1}|} \quad k = 1\ldots(n-1) \tag{21}$$

This formulation normalizes the curvature to have a maximum value of one and a lower bound of zero. Following this normalization, the constant c_w can be interpreted as the mesh density weight for curvature effects relative to unity.

The solution to the variational problem in (20) can be written as (Eggleton, 1971; Crandall et al., 1968)

$$\frac{\mathrm{d}s}{\mathrm{d}q} = \frac{\beta}{c_w \Omega_s'(s) + 1} \tag{22}$$

where β is a constant to be determined. Eq. (22) is a boundary value problem for s with boundary conditions $s=0$ at $q=0$ and $s=L$ at $q=L$. We use the shooting method (Press et al., 1989) and bisection to determine β such that all boundary conditions are satisfied. Bounds on β can be derived by considering the extreme cases $\Omega_s'(s)=0$ and $\Omega_s'(s)=1$. Both conditions lead to a uniform mesh, such that

$$\Omega_s'(s) = 0 \rightarrow \frac{\mathrm{d}s}{\mathrm{d}q} = 1 \rightarrow \beta_{\min} = 1 \tag{23}$$

$$\Omega_s'(s) = 1 \rightarrow \frac{\mathrm{d}s}{\mathrm{d}q} = 1 \rightarrow \beta_{\max} = 1 + c_w \tag{24}$$

With each trial β, we integrate from $q=0$ to $q=L$ using fourth order Runge–Kutta integration. The error function for the bisection is simply $s(q=L)-L$, i.e. the difference between the integrated s coordinate of node n and its known coordinate $s_n=L$. The final step in the process is to recalculate the static solution on the refined mesh, and then use this as the initial configuration for the dynamic calculations.

4. Temporal integration

4.1. Generalized-α method

Gobat and Grosenbaugh (2001a) demonstrated that the box method's temporal discretization scheme has two potential problems related to temporal stability. The method lacks numerical dissipation and suffers from Crank–Nicholson noise. To overcome these deficiencies, Gobat and Grosenbaugh (2001a) adapted the generalized-α method of Chung and Hulbert (1993) to the first-order cable equations. In this method, temporal weighted averaging of the velocity, displacement and force vectors applied to (12) leads to a semi-discrete equation of the form

$$(1-\alpha_m)\tilde{\mathbf{M}}\dot{\mathbf{Y}}^i + \alpha_m\tilde{\mathbf{M}}\dot{\mathbf{Y}}^{i-1} + (1-\alpha_k)\tilde{\mathbf{K}}\mathbf{Y}^i + \alpha_k\tilde{\mathbf{K}}\mathbf{Y}^{i-1} + \tilde{\mathbf{K}}Y + (1-\alpha_k)\tilde{\mathbf{F}}^i + \alpha_k\tilde{\mathbf{F}}^{i-1} = 0 \quad (25)$$

The temporal difference equation is the same as for the generalized trapezoidal rule (Engseth et al., 1988):

$$\mathbf{Y}^i = \mathbf{Y}^{i-1} + \Delta t[(1-\gamma)\dot{\mathbf{Y}}^{i-1} + \gamma\dot{\mathbf{Y}}^i] \quad (26)$$

where Δt is the time step size. The three parameters, α_m, α_k, and γ, together define the generalized-α method. The method is second-order accurate if (Gobat and Grosenbaugh, 2001a)

$$\alpha_m - \alpha_k + \gamma = \frac{1}{2} \quad (27)$$

We can examine the numerical dissipation properties of the algorithm by considering the eigenvalues, $\lambda_{1,2}$, of the amplification matrix and the spectral radius, ρ, which is defined as the maximum absolute value of the eigenvalues. From Gobat and Grosenbaugh (2001a) the spectral radius is

$$\rho = \max|(\lambda_1,\lambda_2)| = \max\left|\frac{1}{2[\gamma\omega\Delta t(\alpha_k-1)+\alpha_m-1]}[2\alpha_m - 1 + (1-\gamma-\alpha_k+2\gamma\alpha_k)\omega\Delta t \pm \sqrt{\omega^2\Delta t^2[(\gamma-1)^2+\alpha_k(\alpha_k+2\gamma-2)] + 2\omega\Delta t[\gamma+2\alpha_m-\alpha_k-1]+1}\right| \quad (28)$$

where ω is frequency. The scheme reduces to a one-parameter algorithm by requiring second-order accuracy through (27) and enforcing the condition that $\lambda_{1,2}$ are both real and equal as $\omega\Delta t$ goes to infinity (Gobat and Grosenbaugh, 2001a). The three parameters of

Table 1
Well-known and one-parameter algorithms that can be implemented using the generalized-α method

Algorithm	α_m	α_k	γ
Box method	0.5	0.5	0.5
Trapezoidal rule	0.0	0.0	0.5
Backward differences	0.0	0.0	1.0
$\lambda^\infty = 0.0$	0.0	-0.5	1.0
$\lambda^\infty = -0.5$	0.167	0.333	0.667
$\lambda^\infty = +0.75$	-6.5	3.0	4.0

the generalized-α method can then be calculated from the following equations:

$$\alpha_k = \frac{\lambda^\infty}{\lambda^\infty - 1}, \alpha_m = \frac{3\lambda^\infty + 1}{2\lambda^\infty - 2}, \gamma = \frac{-1}{\lambda^\infty - 1} \tag{29}$$

where λ^∞ is the value of the double eigenvalue at infinity.

A number of well-known algorithms that can be implemented through the generalized-α method are summarized in Table 1. Spectral radii of these methods as a function of $\omega\Delta t$ are shown in Fig. 1.

The box method with $\lambda^\infty = -1.0$ acts as an all-pass filter with no numerical dissipation. Backward differences with $\lambda^\infty = 0.0$ shows a smooth roll-off at higher frequencies, but is only first-order accurate. A second-order accurate algorithm with $\lambda^\infty = 0.0$ can be specified, but, as with all the second-order accurate algorithms, this algorithm shows a cusp at a frequency where the spectral radius switches (or bifurcates) from being defined by one of the two real eigenvalues to a complex conjugate pair. The trapezoidal rule with unequal eigenvalues at infinity, $\lambda^\infty = (0.0, -1.0)$, behaves as a notch filter with numerical dissipation at the middle frequencies and little dissipation at the highest (undesirable)

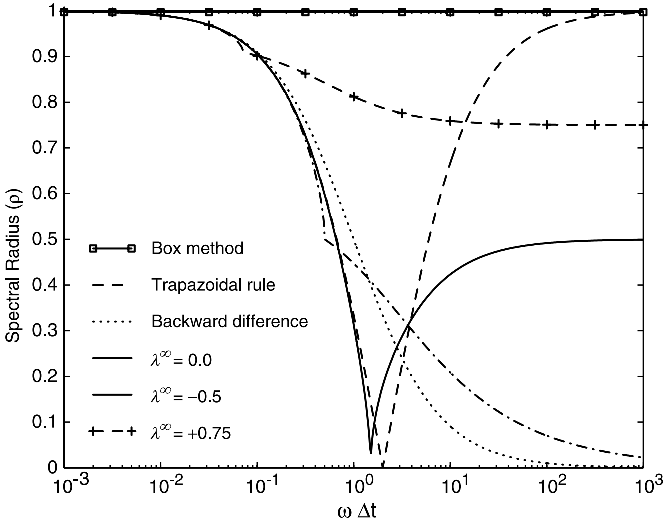

Fig. 1. Spectral radii of a select group from the generalized-α family of algorithms.

frequencies. In this case, the significant increase in spectral radius with increasing frequency after the cusp is due to a second bifurcation that comes from having unequal real eigenvalues at infinity (Gobat and Grosenbaugh, 2001a). If only a single bifurcation is allowed at finite frequencies (i.e. by forcing the eigenvalues to be real and equal at infinity), then the spectral radius either continues to decrease with frequency or, at worst, increases slowly with frequency.

There does not appear to be a clear approach to choosing an optimal value of λ^{∞}. We have found for most cable problems that values between -0.3 and -0.7 yield good results. In our WHOI Cable software, we use a default value of $\lambda^{\infty}=-0.5$.

4.2. Implementation for the nonlinear problem

In (25), the coefficient matrices are written as if they were constant. In the nonlinear problem, the matrices vary in time, and the stability becomes conditional with time. A good choice for avoiding this problem, consistent with the procedure suggested by Hughes (1977) for nonlinear first-order problems, is to calculate average coefficient matrices using the same weights that are used in averaging the velocity and displacement vectors. In this approach, the mass and stiffness matrices at time steps i and $i-1$ are averaged using α_m and α_k, respectively, and the semi-discrete equation becomes (Gobat and Grosenbaugh, 2001a)

$$\begin{aligned}(1-\alpha_m)\tilde{\mathbf{M}}^{\alpha_m}\dot{\mathbf{Y}}^i + \alpha_m\tilde{\mathbf{M}}^{\alpha_m}\dot{\mathbf{Y}}^{i-1} + (1-\alpha_k)\tilde{\mathbf{K}}^{\alpha_k}\mathbf{Y}^i + \alpha_k\tilde{\mathbf{K}}^{\alpha_k}\mathbf{Y}^{i-1} + \tilde{\mathbf{K}}^{\alpha_k}\mathbf{Y}\\ + (1-\alpha_k)\tilde{\mathbf{F}}^i + \alpha_k\tilde{\mathbf{F}}^{i-1} = 0\end{aligned} \tag{30}$$

where

$$\tilde{\mathbf{M}}^{\alpha_m} = (1-\alpha_m)\tilde{\mathbf{M}}^i + \alpha_m\tilde{\mathbf{M}}^{i-1} \tag{31}$$

$$\tilde{\mathbf{K}}^{\alpha_k} = (1-\alpha_k)\tilde{\mathbf{K}}^i + \alpha_k\tilde{\mathbf{K}}^{i-1} \tag{32}$$

4.3. Adaptive time stepping

The stability of the generalized-α method presented above strictly exists only for linear problems. In the nonlinear case, the method cannot guarantee stability because the nonlinear solution procedure at each time step is not unconditionally convergent. Because the nonlinear solver uses the result from the previous time step as the initial guess of the solution for the current time step, the solution at the new time step may not converge if those two solutions are significantly different. For this reason, there are limits to the maximum allowable time step that can successfully be used to propagate the solution in time without giving rise to numerical instabilities.

Typically, we choose a value of Δt based on factors such as the accurate resolution of the physics of the problem, and the desired sampling rate of the numerical solution. Depending on the particular problem, this value of Δt may not be small enough to avoid numerical instabilities that arise over the course of the simulation. This situation is common in cases where the cable goes slack for brief periods of time or when there is rapid lifting and lowering of cable to and from the sea bottom. A procedure for avoiding numerical problems in these cases, without modifying the baseline time step for the whole problem, is adaptive time stepping. If instability arises (i.e. the solution will not converge to a specified tolerance), the time step is reduced automatically to try to get through that portion of the simulation. At each time step where the baseline time increment is not small enough to accurately propagate the solution, Δt is reduced by a factor of ten. The solution then proceeds through ten steps at the smaller increment. The reduction can be recursive, with a practical limit set at four orders of magnitude below the base value of Δt. If the nonlinear solver fails even at this lowest increment, the solution is aborted. This procedure has the advantage that the simulation always produces results on the originally requested sampling grid.

5. Boundary conditions

The discretized governing equations provide only $N\times(n-1)$ equations for the N unknowns at each of the n nodes. The remaining N equations that are needed to completely determine the solution are provided by boundary conditions. The procedures for specifying the boundary conditions for the static and dynamic problems are described below.

5.1. Static problem

For the two-dimensional static problem there are four unknowns at each node. The most common boundary conditions are based on specifying zero curvature at both ends (at nodes 1 and n) and applying a known force at the top end (at node n). Zero curvature is realistic if the cable is attached top and bottom with a joint, shackle, or pivot that releases the moment at the termination. The applied force at the top end comes from environmental and other applied forces (e.g. a tensioning winch) on the platform. The four additional equations, in this case, are

$$\begin{aligned} &\Omega_{31} = 0 \qquad \Omega_{3n} = 0 \qquad F_x - [T_n \cos\phi_n - S_{nn} \sin\phi_n] = 0 \\ &F_y - [T_n \sin\phi_n + S_{nn} \cos\phi_n] = 0 \end{aligned} \tag{33}$$

where F_x and F_y are the applied forces at node n in the global coordinate system.

In many cases, F_x and F_y are not known directly. For oceanographic surface moorings, for example, the interaction between mooring forces and buoy forces are coupled through the buoy draft. Thus, F_x and F_y cannot be known before the problem is solved. For offshore applications, the specified boundary condition is often the position of the platform relative to the anchor, and the forces F_x and F_y are sought as part of the solution. To accommodate these conditions, WHOI Cable iteratively solves the static problem with consecutively better guesses at the top forces until the desired conditions are satisfied.

5.2. Dynamic problem

For the two-dimensional problem with six degrees of freedom per node, we need to formulate a total of six boundary conditions at the two ends. Like the static problem, releasing moments at the two terminations provides two equations. At the anchor, we simply impose no motion by setting both normal and tangential velocities to zero. At the top, we can impose either time-varying forces or velocities in the two global directions. Specifying velocities is the more common case, as we are typically interested in the response of the system to a specified environmentally induced motion of the top of the mooring. In this case, the six boundary conditions are

$$\begin{aligned} &\Omega_{31}^i = 0 \qquad \Omega_{3n}^i = 0 \qquad u_1^i = 0 \qquad v_1^i = 0 \\ &U_n^i - [u_n^i \cos\phi_n^i - v_n^i \sin\phi_n^i] = 0 \qquad V_n^i - [u_n^i \sin\phi_n^i + v_n^i \cos\phi_n^i] = 0 \end{aligned} \tag{34}$$

where U_n^i and V_n^i are the specified velocities at time step i and node n in the global vertical and horizontal directions, respectively. In a towing problem, the no-motion constraint at the anchor is replaced with a force balance between cable tension and shear and hydrodynamic and thrust forces on the tow body.

5.3. Bottom interaction

Following the same approach as Webster (1995), the unilateral boundary condition at the sea floor is modeled as an elastic foundation with linear stiffness and damping properties. Given the vertical coordinate of the bottom y_{bot}, which may vary with horizontal position, the bottom exerts a force on node j if $y_j \leq y_{bot}$. For both static and dynamic problems, the force is defined as

$$F_{\text{bot}} = k(y_j - y_{\text{bot}}) \tag{35}$$

where k is the stiffness per unit length of the bottom. In static problems, the force is constrained so that $F_{\text{bot}} \leq w_o$. The force is always assumed to act in the global vertical direction and as such can be treated simply as a modification to the wet weight w_o in the governing equations. In the dynamic problem, we also add a damping force

$$F_{\text{damp}} = -bv_j \tag{36}$$

where b is the dashpot constant of the bottom and v_j is the normal velocity of node j. For most problems the gross response of the system is largely insensitive to the choice of k and b.

The advantages of this treatment of the bottom are the simplicity with which it can be implemented and the generality which it allows. The approach places no restrictions on the number of touchdown points or where and how those points move during the dynamic problem because the entire mooring, including grounded line, is always 'in play'. This contrasts with approaches, which track a single touchdown point, adding or removing line from the problem to calculate a dynamic response only for line that is instantaneously above that point. The implementation described above has no difficulty handling cases in which positively buoyant portions of the line float above the bottom between heavier portions of grounded line, for example.

6. Nonlinear solver

Both static and dynamic cable problems can be generalized as a system of first-order nonlinear partial differential equations

$$\frac{\partial \mathbf{Y}}{\partial s} + \mathbf{Q}(s, \mathbf{Y}) = 0 \tag{37}$$

where at each time step, the dynamic problem represents a quasi-static equilibrium problem. $\mathbf{Y}$ is an $N\times 1$ vector of the dependent variables and $\mathbf{Q}$ is a vector that includes the effects of environmental forcing, damping, and inertia. When discretized and combined with N boundary conditions, (40) represents a coupled system of $N\times n$ nonlinear equations for $N\times n$ unknowns. At each time step we solve for $\mathbf{Y}$ iteratively, using a nonlinear relaxation procedure (Press et al., 1989; Gobat, 2000). Given an initial guess, $\mathbf{Y}^0$, we calculate successively better approximations, $\mathbf{Y}^{\boldsymbol{k}}$, through an update vector, $\Delta\mathbf{Y}^{\boldsymbol{k}}$, and a relaxation factor, μ

$$\mathbf{Y}^{k+1} = \mathbf{Y}^k + \mu\Delta\mathbf{Y}^k \tag{38}$$

The purpose of the relaxation factor is to slow (for $0<\mu<1$) the update in cases of strong nonlinearity. The iterative updates of $\mathbf{Y}^{\mathrm{k}}$ continue until the updates become sufficiently small as to not warrant continuation of the process. The total error at each iteration, $(^{k}, used to make this determination is defined as

$$\sigma^k = \frac{1}{Nn}\sum_{m=1}^{N}\frac{1}{\chi_m}\sum_{j=1}^{n}\Delta\mathbf{Y}_{j,m}^k \tag{39}$$

where $\Delta\mathbf{Y}_{j,m}^k$ are the N components of the update vector at node j and iteration k and $(_m$ are scaling constants appropriate to each of the physical variables represented within $\mathbf{Y}$.

In many cases, it is desirable to have the relaxation factor vary as the solution progresses. This is particularly true in the static solution of some problems, which may need fine movement of the relaxation process as the solution approaches equilibrium. For example, for cable resting on the sea floor, the resolution of the location of the touchdown point can be difficult to resolve because of the unilateral nonlinearity represented by the bottom. With too large a relaxation factor the update might pull a substantial amount of cable off the bottom, only to be followed by an update that drops too much back onto the bottom.

To accommodate this behavior, the actual relaxation factor used from iteration to iteration is varied according to the progress of the solution. If at any point during the solution, the size of the update increases from one step to the next, $\sigma^{k+1}>\sigma^k$, the relaxation factor applied to the update at that step is reduced from the factor used at the previous step

$$\sigma^{k+1} > \sigma^k \rightarrow \mu^{k+1} = \frac{\mu^k}{R_1} \tag{40}$$

where R_1 is a positive constant greater than unity. If the error is decreasing as it should, then we take the opposite approach and try to speed the solution by increasing the relaxation factor

$$\sigma^{k+1} < \sigma^k \rightarrow \mu^{k+1} = R_2\mu^k \tag{41}$$

where $1<R_2<R_1$. The relaxation factor is not allowed to increase beyond the user specified baseline value, μ_0, and, as a protection against becoming too small, is not allowed to decrease beyond $\mu_0/1000$. In WHOI Cable, $R_1=1.1$ and $R_{1=}1.02$. The adaptive procedure has the effect of driving the relaxation factor into an equilibrium at which the solution can make the best progress—if the baseline relaxation factor is too large and the solution starts to diverge, the relaxation factor is reduced until the solution begins to converge. The relaxation factor is prevented from remaining too small by (41). This procedure still requires a reasonable value for the starting relaxation factor. However, it avoids having to set the relaxation factor low when a small value is only needed for a portion of the solution procedure. For problems with cable on the sea floor, the last part of the solution may require relaxation factors on the order of 10^{-3}, but may proceed quite well in the initial iterations with $\mu=10^{-1}$. An example of the error progress during such a problem is shown in Fig. 2. In the upper panel, the solid line shows the error in a solution with a starting relaxation of 0.2. The bottom panel shows how the relaxation factor changes, for the adaptive solution, as the solution progresses. The dashed line in the upper panel shows the error in a solution with a constant relaxation of 0.004 (this is the largest constant relaxation factor that results in a solution convergent to $\sigma=0.001$). Not only does the adaptive procedure save a significant amount of trial and error to determine an appropriate relaxation constant, but it also reduces the number of iterations by more than a factor of two.

6.1. Coordinate integration

The solution procedure calculates the $N\times n$ dependent variables that are explicitly included in the governing equations. Because both static and dynamic governing equations in the formulation described above do not explicitly include the coordinate positions of the nodes, these positions must be calculated in a separate procedure. The position of the nodes is critical to the solution. Bottom boundary effects, wave forces, and current are all dependent on spatial position. For this reason, the coordinate positions of all the nodes are updated at each iteration through integration using

$$x(s) = \int_0^s (1+\varepsilon)\cos\phi \, \mathrm{d}s \qquad y(s) = \int_0^s (1+\varepsilon)\sin\phi \, \mathrm{d}s \tag{42}$$

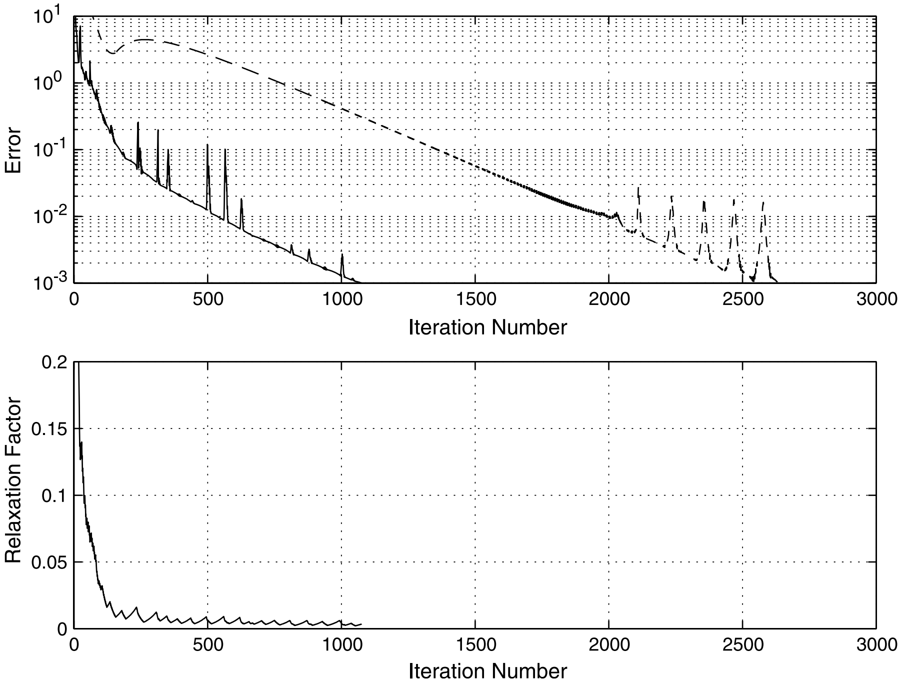

Fig. 2. Top panel shows the error during the static solution of a mooring problem with bottom interaction. The dashed line corresponds to a solution achieved using the largest constant relaxation factor (0.004) that will result in convergence to an error level of 0.001. The solid line is the error for a solution using the adaptive procedure described in the text. Bottom panel shows the instantaneous value of the relaxation factor corresponding to the adaptive solution.

7. Applications

We present the results from problems involving a towed, a deepwater oceanographic mooring, and an all-chain, shallow-water mooring. In particular, we compare performance of the various time-integration methods that can be recovered from the generalized-α method. These include the box method of Ablow and Schechter (1983) and the backward difference method of Koh et al. (1999). Adaptive time stepping and adaptive relaxation were enabled for all the simulations. A uniform mesh density was used for the towing and deep-water mooring examples. Results using a uniform mesh and one constructed using adaptive spatial discretization were compared for the all-chain, shallow-water mooring example.

7.1. Towed horizontal array

We used WHOI Cable to simulate a high-speed circular maneuver of a towed horizontal array that was first presented by Ablow and Schechter (1983) to verify their TCABLE program. The simulated maneuver involved a tow-ship traveling at a constant

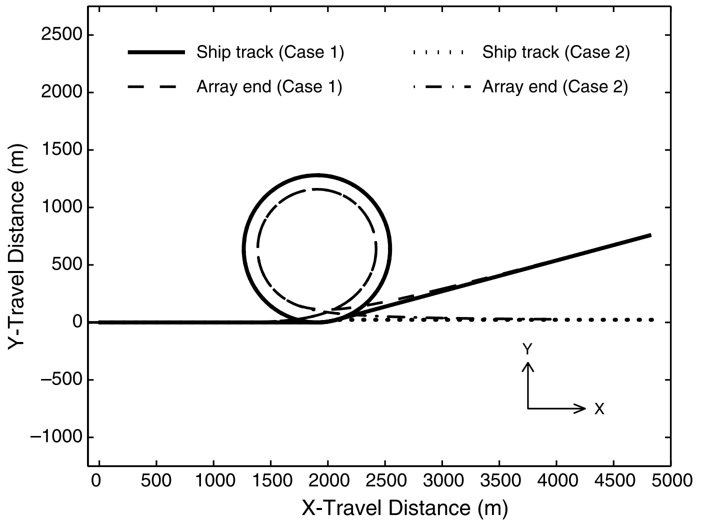

Fig. 3. Prescribed ship track and position of array end for the simulation of a 375° circular maneuver of a towed horizontal array. For Case 1, the ship track is always tangent to the circle. For Case 2, the ship track returns impulsively to its original direction of 0° after the 375° turn is completed.

speed of 9.52 m/s (18.5 knots) and initially going straight ahead. This straight-ahead motion was simulated for 200 s (though Ablow and Schechter simulated this portion of the maneuver for only one second). The straight-ahead motion was immediately followed by a 375° circular turn with a radius of 640 m. The circular motion lasted for 440 s and ended with the ship traveling straight ahead on a course of 15° measured counterclockwise from the initial heading (Fig. 3). The final straight-ahead motion was simulated for 300 s at which time the system was nearly back to equilibrium. The geometry, wet weight, and fluid drag coefficients of the simulated system followed directly from Ablow and Schechter (1983). A 723-m negatively buoyant tow cable extended from the ship down to a 273.9-m neutrally buoyant horizontal array. Attached to the other end of the array was a 30.5-m 'rope drogue', which was slightly negatively buoyant. We estimated values for the mass, added mass, elastic stiffness EA, bending, and torsional stiffness. The exact physical parameters used in our simulation are given in the Appendix. Uniform node spacing of 1 m was used in all simulations.

Fig. 4 shows results obtained using WHOI Cable and TCABLE for the depth of the horizontal array at a point 8.2 m from the bottom end of the tow cable. This point is referred to as 'Point A' in Ablow & Schechter (1983). While the comparison is not exact, it is quite good considering our inclusion of bending stiffness, possible differences in material properties, and numerical differences arising from the differing solution procedures. For example, Ablow and Schechter (1983) reported using a time step of 20 s for the turning sections of the maneuver, while WHOI Cable adapted down to a 2-s time step on a number of occasions during the turn. We note that Buckham and Nahon (2001) also reported using very small time steps when they incorporated bending and torsional stiffness in a lumped-mass method.

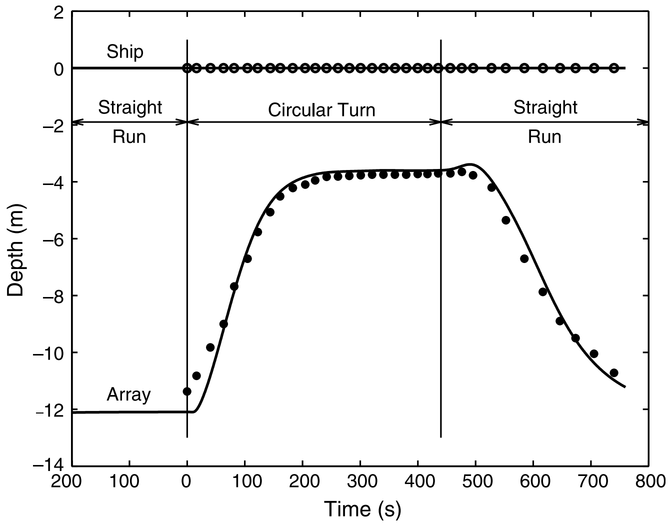

Fig. 4. Depth of horizontal array measured at a point 8.2 m downstream from the head of the array for constant ship speed of 9.52 m/s (18.5 knots). WHOI Cable results (solid lines) are compared with the results of Ablow and Schechter (1983) (symbols).

In simulating the previously described turning maneuver, we found that the results were invariant to changes in the time-integration scheme (e.g. the box method gave the same result as other generalized-α schemes with numerical dissipation). This is not always the case. We modified slightly the turning maneuver by having the ship immediately turn back to its original course of 0° at the moment it completed the 375° turn (Fig. 3). This introduced a sudden change in cable tension that resulted in the formation of Crank–Nicholson noise for the box method (Fig. 5). This was not observed for integration schemes that contained numerical damping—in this case for $\lambda^{\infty} = -0.5$. Similar results were achieved for other methods that had numerical dissipation including methods with λ^{∞} between 0.0 and -0.7 as well as backward differences.

7.2. Inverse catenary deepwater mooring

In this example, we calculated the dynamic tension at the top of an oceanographic mooring used to link a sea floor observatory with the sea surface. The mooring (Fig. 6) consisted of a continuous electro-optical-mechanical (EOM) cable that had armor sheathing over the top 750 m and Vectran sheathing over the lower portion. The cable was elastically stiff in order to prevent excess stretching of the optical fibers that ran up and down the middle of the cable. Compliancy was incorporated into the mooring by having a scope of about 1.2 and placing, at the top of the mooring, a 16-m rubber 'snubber' hose in which the electrical wires and optical fibers were coiled (Paul et al., 1999). Football-shaped cable floats were attached to the armored section of the cable to reduce mean loads in the snubber hose. Cable floats were also attached to the lower section of the EOM cable in order to keep excess cable from lying on the sea bottom in low or slack currents. Under slack conditions, the lower part of the mooring line

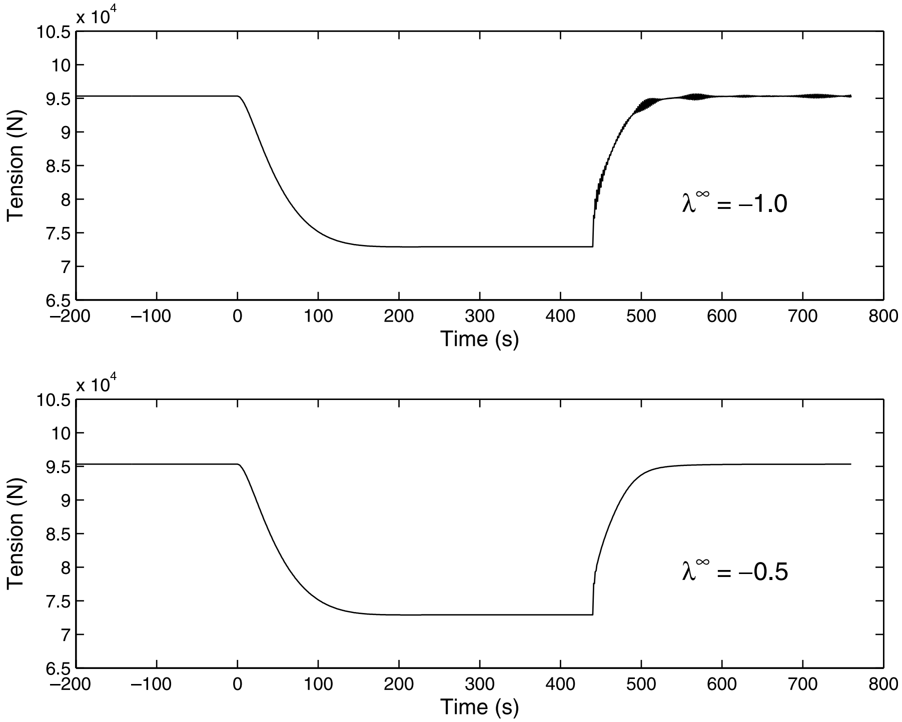

Fig. 5. Simulated tow cable tension at the ship for Case 2 of the towed array example. Top panel shows the simulated tension record using the box method ($\lambda^{\infty} = -1.0$). Bottom panel shows the simulated tension record using generalized-α scheme with numerical dissipation ($\lambda^{\infty} = -0.5$).

takes the shape of an '*S*' lying on its side with the top loop of the '*S*' located well below the sea surface and the bottom loop of the '*S*' located well above the sea bottom. The material properties of the mooring, which were used as input in WHOI Cable, are given in the Appendix. Moorings similar to this are being used by Monterey Bay Aquarium Research Institute (MBARI) for use in ocean observing systems (Chaffey et al., 2001) and have been analyzed in detail by Han and Grosenbaugh to appear.

For this comparison, we chose environmental conditions that corresponded to a deployment site in Monterey Bay where the water depth was 1860 m. A sea state with a significant wave height of 9.8 m and peak period of 16 s was used for dynamic forcing. The sea state corresponds to the 25-year return storm for Monterey Bay, which was determined from historical wave height measurements made by a nearby National Data Buoy Center surface mooring (Station 46042). The current profile used in the simulations is given in Table 2 and is based on actual measurements that were made near the proposed site (Chaffey et al., 2001). A steady wind speed of 20 m/s was used to calculate wind load on the surface buoy. Simulations were performed with the numerical parameter set to two different values: $\lambda^{\infty} = -1.0$ (box method) and $\lambda^{\infty} = -0.5$. Each simulation was run for 600 s. Comparisons between the different values of λ^{∞} were made regarding how quickly convergence was achieved and how quickly the simulations ran in real time. The initial

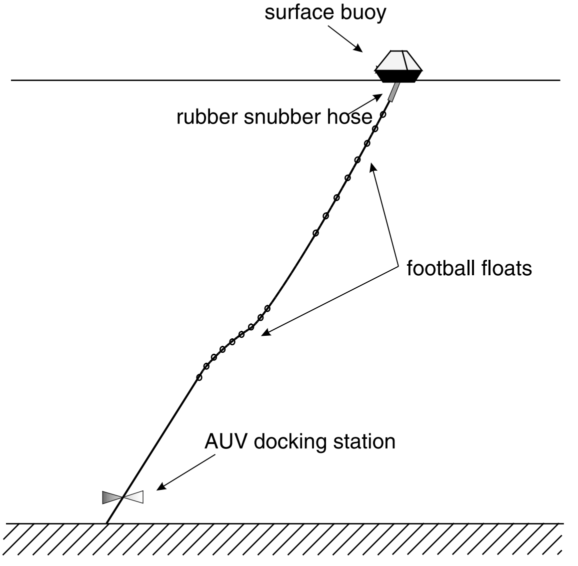

Fig. 6. Deepwater oceanographic S-tether mooring made with a relatively stiff electro-optical-mechanical mooring cable.

time step for the simulations was 0.5 s, which was eventually reduced to 0.01 s. Uniform node spacing of 1 m was used in the chain and snubber sections. Uniform node spacing of 10 m was used in the EOM cable sections.

The results of the simulations using a base time step equal to 0.5 s are given in Fig. 7. The results for $\lambda^{\infty} = -1.0$ (box method) show an upward drift of the mean tension for the initial 370 s and then a slow oscillation about a mean value that is over twice the actual converged static tension. The average value of the mean tension for this case (averaged over 600 s) is 16,340 N. The actual mean tension should be equal to the static tension of 8350 N since the surface buoy was allowed to move only in the vertical direction. Also, the standard deviation of the tension, which is equal to 3410 N, is considerably greater than the converged value of 2910 N. The results using $\lambda^{\infty} = -0.5$ show a very small upward bias in the mean tension, which averaged over the length of the simulation, gives a value of

Table 2
Current profile for monterey bay

Depth (m)	Current speed (m/s)
0	0.70
50	0.63
100	0.56
150	0.50
200	0.50
250	0.45
300	0.25
1860	0.12

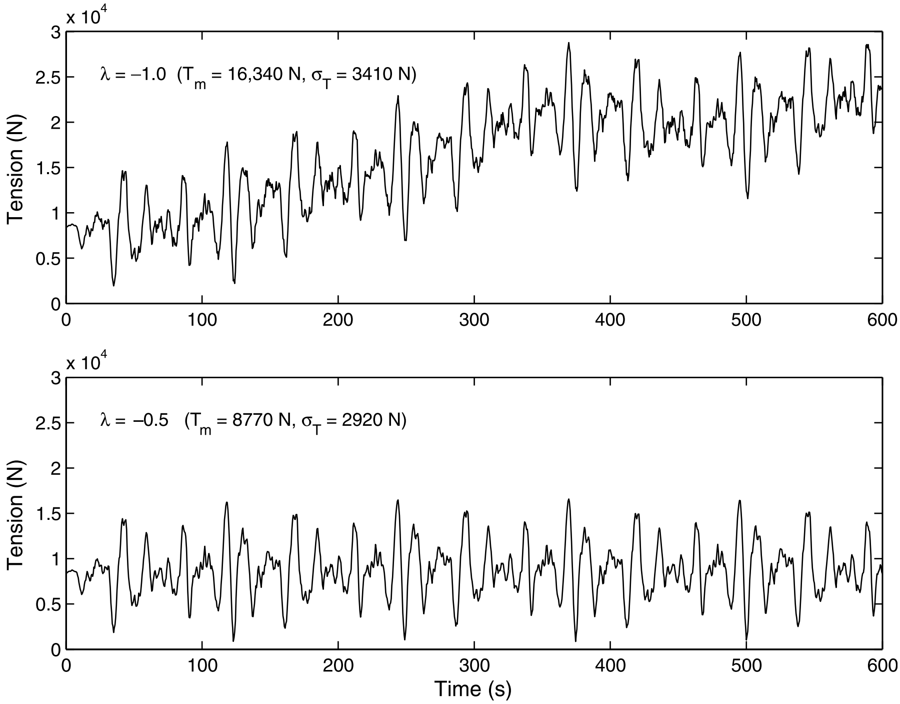

Fig. 7. Time series of the tension at the surface buoy of the deepwater oceanographic mooring for $\lambda^{\infty}=-1.0$ (box method) and $\lambda^{\infty}=-0.5$. The base time step was 0.5 s. The values in parentheses (T_m, σ_T) represent the mean tension averaged over the length of the simulation and the standard deviation. The converged values (see text) for T_m and σ_T are 8350 N and 2910 N, respectively.

8770 N. The standard deviation for this case is 2920 N. The box method ($\lambda^{\infty}=-1.0$) converges at a base time step of 0.02 s while algorithm with $\lambda=-0.5$ converges for a base time step of 0.2 s. For time step size of 0.1 s, the computational effort for the box method ($\lambda^{\infty}=-1.0$) was as much as 30% greater than for the algorithm with $\lambda^{\infty}=-0.5$. This is primarily due to the box method having to adapt more often to smaller time steps during the computations, especially when a relatively large baseline time step was used.

The computations using values of λ^{∞} between -0.3 and -0.7 gave similarly good results. However, for backwards differences, the mean tension increased slightly (by about 20%) over the course of the 600 s simulation with a time-step of 0.5. This bias was eliminated for a time step of 0.02 s (or less). Computations using the second-order accurate algorithm of $\lambda^{\infty}=0.0$, gave slightly better results than backward differences in terms of the original bias (about 15%) and convergence (at time step = 0.05 s).

7.3. All-chain, shallow-water mooring

In the final example, we consider the problem of an all-chain, shallow-water oceanographic mooring in a uniform current with an imposed sinusoidal vertical velocity

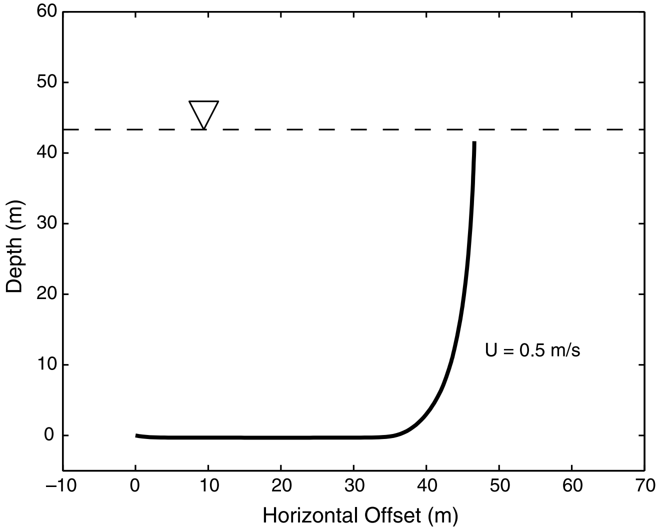

Fig. 8. Static configuration of the all-chain, shallow-water mooring in 0.5 m/s uniform current.

at the top node of the mooring. The physical characteristics of the mooring are given in the Appendix. The static configuration in a uniform current of 0.5 m/s is shown in Fig. 8. The difficulty with this simulation involves the interaction between the chain and the sea bottom (Gobat and Grosenbaugh, 2001b). As we show, this simulation can breakdown without the introduction of some numerical dissipation.

We tested three forms of the algorithm: the box method ($\lambda^{\infty} = -1.0$), backward differences, and the generalized-α method with $\lambda^{\infty} = -0.5$. The simulations were run for a maximum of 300 s (base time step = 0.1 s) with an imposed vertical motion of amplitude 2.0 m and period 8.0 s. The time series for the total tension at the top node are given in Fig. 9.

There is a start-up transient in all cases. For the box method, the transient continues to grow, fed by high-frequency energy caused by the chain contacting the sea bottom, until the simulation fails due to the adaptive time-stepping scheme reaching its prescribed limit. For backward differences and the algorithm with $\lambda^{\infty} = -0.5$, the initial transient dies out and thesimulations proceed to completion. The results corresponding to backward differences show a steady increase in the value of the peak tension (due to the algorithm being only first-order accurate), though the solution remains stable due to numerical dissipation. Only the algorithm $\lambda^{\infty} = -0.5$, which combines second-order accuracy with numerical dissipation, produces a stable and consistent solution.

The above results for the shallow-water mooring were obtained using uniform spaced nodes, 0.5 m apart. We reran the simulations using the adaptive discretization feature of WHOI Cable with a weighting constant $c_w = 20$. The results obtained on the adaptively refined mesh were similar to those in Fig. 9 except there was a significant reduction in the amplitude of numerical noise, which occurred in the troughs of the tension signal when the chain contacted the bottom. Also, the mean tensions of the mooring line near

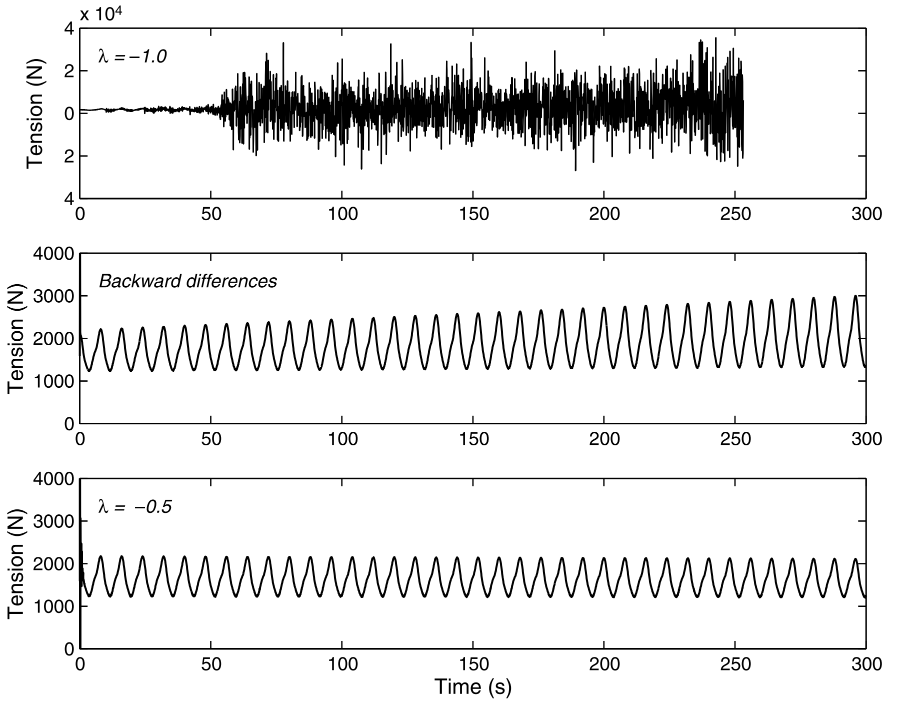

Fig. 9. Total tension at the top node (surface buoy) of the all-chain, shallow-water mooring for $\lambda^{\infty} = -1.0$ (box method), backward differences, and $\lambda^{\infty} = -0.5$. The base time step was 0.1 s.

the touchdown region increased by nearly 6% when adaptive discretization was enabled. A solution with uniform node spacing converged to the solution with adaptive discretization after the mesh density was increased by a factor of four, which increased the computation time, also, by a factor of four.

A detailed analysis of the errors associated with the numerical simulation of this mooring in a uniform current of 2.0 m/s is presented in Gobat and Grosenbaugh (2001a).

8. Summary

The computer method presented in this paper for analyzing the dynamics of ocean cable systems contains a number of features that are aimed at increasing stability, accuracy, and usability. The inclusion of bending stiffness in the mathematical equations allows for the simulation of low-tension effects. Adaptive time stepping, adaptive gridding, and adaptive relaxation greatly aid users in obtaining solutions in a timely manner. Most importantly, the addition of the generalized-α time-integration scheme retains second-order accuracy in time while controlling high-frequency numerical noise through the addition of numerical dissipation. Improved stability is also achieved through the averaging of coefficient matrices.

Acknowledgements

This research was supported by the Office of Naval Research (Ocean Engineering and Marine Systems) under grants N00014-92-J-1269 and N00014-04-10030.

Appendix A

A.1. Configuration of towed horizontal array (starting with the ship)

- Ship
- 723 m 1.6-inch tow cable
- 273.9 m 3.125-inch array
- 30.5 m 1-inch rope drogue

Cable properties	Tow cable	Horizontal array	Rope drogue
EA (N)	1×10^8	1×10^8	5×10^6
EI (Nm^2)	1000	1000	0.01
GJ (Nm^2)	50	50	0.01
Mass/length (kg/m)	2.37	5.07	0.58
Added mass/length (kg/m)	1.33	5.07	0.52
Wet weight/length (N/m)	2.33	0.0	0.57
Diameter (m)	0.041	0.079	0.025
C_{dn}[a]	2.0	1.8	1.8
C_{dt}[b]	0.015	0.009	0.022

[a] C_{dn} is the normal drag coefficient.
[b] C_{dt} is the tangential drag coefficient.

A.2. Configuration of deepwater oceanographic mooring (starting at the anchor)

- Anchor
- 5 m ½-inch trawler chain
- 30 m Vectran EOM cable
- AUV docking station
- 15 m Vectran EOM cable with three *large-sized* cable floats attached every 5 m starting at the lower end
- 235 m Vectran EOM cable
- 80 m Vectran EOM cable with five *large-sized* cable floats attached every 20 m starting at the lower end
- 1050 m Vectran EOM cable
- Termination between Vectran and armored EOM cable potted in urethane with 3 m ½-inch trawler chain
- 750 m armored EOM cable with 17 *medium-sized* cable floats attached every 40 m starting 40 m up from the lower end

- Two 8 m snubber hoses (total length 16 m) joined together by steel coupling
- Surface buoy

Cable properties	Vectran EOM cable	Armored EOM cable	Snubber hose
EA (N)	5×10^6	1×10^7	3×10^4
EI (Nm^2)	0.14	0.5	1000
GJ (Nm^2)	0.1	0.3	500
Mass/length (kg/m)	0.47	0.85	17.00
Added mass/length (kg/m)	0.34	0.55	14.33
Wet weight/length (N/m)	1.49	2.98	21.96
Diameter (m)	0.0206	0.0262	0.1334
C_{dn}	2.0	1.5	1.5
C_{dt}	0.01	0.01	0.01

Float properties	Medium-sized cable float	Large-sized cable float
Equivalent diameter[a] (m)	0.45	0.58
Mass (kg)	18.5	37.9
Added mass (kg)	14.8	31.8
Wet weight (N)	−110.8	−214.8
C_{dn}	1.0	1.0
C_{dt}	0.2	0.2

[a]Equivalent diameter is the diameter of a sphere that provides the same normal projected area as the actual float.

A.3. Configuration of all-chain, shallow-water oceanographic mooring (starting at the anchor)

- Anchor
- 45.0 m ½-inch trawler chain
- ‘AxPack’ (0.76 m long cylindrical pressure housing with accelerometers)
- 3.5 m ½-inch trawler chain
- ‘AxPack’
- 7.0 m ½-inch trawler chain
- ‘AxPack’
- 23.0 m ½-inch trawler chain
- Surface buoy

Cable properties	½-Inch trawler chain	AxPack[a]
EA (N)	6.44×10^7	8.0×10^7
EI (Nm^2)	10.0	3.0×10^4
GJ (Nm^2)	0.1	0.1
Mass/length (kg/m)	3.73	10.02
Added mass/length (kg/m)	0.48	4.67
Wet weight/length (N/m)	31.85	70.82
Diameter (m)	0.0495	0.0762

Cable properties	½-Inch trawler chain	AxPack[a]
C_{dn}	0.5	0.8
C_{dt}	0.05	0.065

[a]The AxPack is a 0.76-m long cylindrical pressure housing that is mounted in-line and treated as part of the mooring with equivalent cable properties.

References

Ablow, C.M., Schechter, S., 1983. Numerical simulation of undersea cable dynamics. Ocean Engineering 10, 443–457.

Buckham, B., Nahon, M., 2001. Formulation and validation of a lumped mass model for low-tension ROV tethers. International Journal of Offshore and Polar Engineering 11, 282–289.

Burgess, J.J., 1993. Bending stiffness in a simulation of undersea cable deployment. International Journal of Offshore and Polar Engineering 3, 197–204.

Chaffey, M., Mellinger, E., Paul, W., 2001. Communications and power to the seafloor: MBARI's ocean observing system mooring concept. In: Oceans, pp. 2473–2481.

Chatjigeorgiou, I.K., Mavrakos, S.A., 1999. Comparison of numerical methods for predicting the dynamic behavior of mooring lines. In: Proceedings of the Ninth International Offshore and Polar Engineering Conference, Brest, France.

Chiou, R.B., Leonard, J.W., 1991. Nonlinear hydrodynamic response of curved singly-connected cables. In: Computer Modelling in Ocean Engineering. Balkema, Rotterdam.

Chung, J., Hulbert, G., 1993. A time integration algorithm for structural dynamics with improved numerical dissipation. Journal of Applied Mechanics 60, 371–375.

Crandall, S.H., Karnopp, D.C., Kurtz Jr.., E.F., Pridmore-Brown, D.C., 1968. Dynamics of Mechanical and Electromechanical Systems. Krieger, Malabar, ML.

Delmer, T.N., Stephens, T.C., Coe, J.M., 1983. Numerical simulation of towed cables. Ocean Engineering 10, 119–132.

Eggleton, P.P., 1971. The evolution of low mass stars. Monthly Notices of the Royal Astronomical Society 151, 351–364.

Engseth, A., Bech, A., Larsen, C.M., 1988. Efficient method for analysis of flexible risers. In: Proceedings of Behavior of Offshore Structures, pp. 1357–1371.

Garrett, D.L., 1982. Dynamic analysis of slender rods. Journal of Energy Resources Technology 104, 302–306.

Gobat, J.I., 2000. The dynamics of geometrically compliant mooring systems. PhD Dissertation, Massachusetts Institute of Technology and Woods Hole Oceanographic Institution Joint Program, Woods Hole, MA.

Gobat, J.I., Grosenbaugh, M.A., 2001a. Applications of the generalized-α method to the time integration of the cable dynamics equations. Computer Methods in Applied Mechanics and Engineering 190, 4817–4829.

Gobat, J.I., Grosenbaugh, M.A., 2001b. Dynamics in the touchdown region of catenary moorings. International Journal of Offshore and Polar Engineering 11, 273–281.

Han, S., Grosenbaugh, M., to appear. On the design of single-point cable-linked moorings for ocean observatories. IEEE Journal of Oceanic Engineering.

Hoff, C., Pahl, P.J., 1988. Development of an implicit method with numerical dissipation from a generalized single-step algorithm for structural dynamics. Computer Methods in Applied Mechanics and Engineering 67, 367–385.

Howell, C.T., 1992. Investigation of the dynamics of low-tension cables. PhD Dissertation, Massachusetts Institute of Technology and Woods Hole Oceanographic Institution Joint Program, Woods Hole, MA.

Huang, S., 1994. Dynamic analysis of three-dimensional marine cables. Ocean Engineering 21, 587–605.

Hughes, T.J.R., 1977. Unconditionally stable algorithms for nonlinear heat conduction. Computer Methods in Applied Mechanics and Engineering 10, 135–139.

Hughes, T.J.R., Belytschko, T., 1983. A precis of developments in computational methods for transient analysis. Journal of Applied Mechanics 50, 1033–1041.

Koh, C.G., Zhang, Y., Quek, S.T., 1999. Low-tension cable dynamics: numerical and experimental studies. Journal of Engineering Mechanics 125, 347–354.

Larsen, C.M., 1992. Flexible riser analysis—comparison of results from computer programs. Marine Structures 5, 107–119.

Leonard, J.W., Nath, J.H., 1981. Comparison of finite element and lumped parameter methods for oceanic cables. Engineering Structures 3, 153–167.

McNamara, J.F., O'Brien, P.J., Gilroy, S.G., 1986. Nonlinear analysis of flexible risers using hybrid finite elements. In: Proceedings of Fifth International Conference on Offshore Mechanics and Arctic Engineering, Tokyo, vol. 3, pp. 371–377.

Milinazzo, F., Wilkie, M., Latchman, S.A., 1987. An efficient algorithm for simulating the dynamics of towed cable systems. Ocean Engineering 14, 513–526.

Newmark, N.M., 1959. A method of computation for structural dynamics. ASCE Journal of the Engineering Mechanics Division 85, 67–94.

Park, K.C., 1975. Evaluating time integration methods for nonlinear dynamic analysis. In: Belytschko, T., Osias, J.R., Marcal, P.V. (Eds.), Finite Element Analysis of Transient Non-Linear Behavior Applied Mechanics Symposia Series. ASME, New York, pp. 35–58.

Park, H.I., Jung, D.H., Koterayama, W., 2003. A numerical and experimental study on dynamics of a towed low tension cable. Applied Ocean Research, 289–299.

Paul, W., Irish, J., Gobat, J., Grosenbaugh, M., 1999. Coastal mooring design: taut elastomeric and chain catenary surface buoy moorings. In: Oceans '99, pp. 419–426.

Paulling, J.R., Webster, W.C., 1986. A consistent, large-amplitude analysis of the coupled response of a TLP and tendon system. In: Proceedings of Fifth International Conference on Offshore Mechanics and Arctic Engineering, Tokyo, vol. 3, pp. 126–133.

Polachek, H., Walton, T.S., Mejia, R., Dawson, C., 1963. Transient motion of an elastic cable immersed in a fluid. Mathematics of Computation 17, 60–63.

Press, W.H., Flannery, B.P., Teukolsky, S.A., Vetterling, W.T., 1989. Numerical Recipes in C: The Art of Scientific Computing. Cambridge University Press, Cambridge.

Sanders, J.V., 1982. A three-dimensional dynamic analysis of a towed system. Ocean Engineering 9, 483–499.

Sun, Y., Leonard, J.W., Chiou, R.B., 1994. Simulation of unsteady oceanic cable deployment by direct integration with suppression. Ocean Engineering 21, 243–256.

Thomas, D.O., 1993. A numerical investigation of time integration schemes applied to the dynamic solution of mooring lines, PhD dissertation, The University of Newcastle upon Tyne, Newcastle, UK.

Thomas, D.O., Hearn, G.E., 1994. Deepwater mooring line dynamics with emphasis on seabed interference effects. In: Proceedings of the 26th Offshore Technology Conference, Houston TX, pp. 203–214.

Tjavaras, A.A., 1996. Dynamics of highly extensible cables. PhD dissertation, Massachusetts Institute of Technology Cambridge, MA.

Walton, T.S., Polachek, H., 1960. Calculation of transient motion of submerged cables. Mathematics of Computation 14, 27–46.

Webster, W.C., 1995. Mooring induced damping. Ocean Engineering 22, 571–591.

Wood, W.L., 1990. Practical Time-Stepping Schemes. Clarendon Press, Oxford.

Zienkiewicz, O.C., Wood, W.L., Hine, N.W., 1984. A unified set of single step algorithms part 1: general formulation and applications. International Journal for Numerical Methods in Engineering 20, 1529–1552.

Zueck, R.F., 1997. Local/global approach to nonlinear simulation of compliant marine structures. Technical Report TR-2073-OCN, Naval Facilities Engineering Service Center, Port Hueneme, CA.